



HAL
open science

Effect of Bubble Nuclei Characteristics on a Cavitating Hydrofoil: Numerical Investigation with Homogeneous Cavitation Model

Wakana Tsuru, Shin-Ichi Tsuda, Satoshi Watanabe

► **To cite this version:**

Wakana Tsuru, Shin-Ichi Tsuda, Satoshi Watanabe. Effect of Bubble Nuclei Characteristics on a Cavitating Hydrofoil: Numerical Investigation with Homogeneous Cavitation Model. International Symposium on Transport Phenomena and Dynamics of Rotating Machinery (ISROMAC 2017), Dec 2017, Maui, United States. hal-02349552

HAL Id: hal-02349552

<https://hal.science/hal-02349552>

Submitted on 5 Nov 2019

HAL is a multi-disciplinary open access archive for the deposit and dissemination of scientific research documents, whether they are published or not. The documents may come from teaching and research institutions in France or abroad, or from public or private research centers.

L'archive ouverte pluridisciplinaire **HAL**, est destinée au dépôt et à la diffusion de documents scientifiques de niveau recherche, publiés ou non, émanant des établissements d'enseignement et de recherche français ou étrangers, des laboratoires publics ou privés.

Effect of Bubble Nuclei Characteristics on a Cavitating Hydrofoil: Numerical Investigation with Homogeneous Cavitation Model

Wakana Tsuru^{1*}, Shin-ichi Tsuda², Satoshi Watanabe²



Abstract

The aim of this study is to clarify the effects of number density and initial diameter of bubble nuclei on global behavior of cavitating flow around an isolated Clark Y hydrofoil in numerical simulation. Measurements of the number density distributions of bubble nuclei are carried out, then the number density and averaged diameter of bubble nuclei are calculated from the measurement results and are used for the parameters of cavitation models in the numerical analysis. The numerical results are compared with those obtained with defaulted values provided by a solver. As a result, it is confirmed that the number density of bubble nuclei affects time-averaged pressure distribution on the blade surface, and the fluctuation of the lift coefficient and the cavitation area. In addition, the location of the cavity leading edge in the case of using the parameters obtained by the measurements moves apparently downstream, resulting in a better agreement with actual one.

Keywords

Homogeneous cavitation model — Bubble nuclei — Clark Y hydrofoil

¹Graduate School of Engineering, Kyushu University, Japan

²Department of Mechanical Engineering, Kyushu University, Japan

*Corresponding author: tsuru.w.123@s.kyushu-u.ac.jp

INTRODUCTION

In development stage of fluid machinery, numerical simulations for cavitating flow by CFD (Computational Fluid Dynamics) are widely performed. In the cavitation simulation, since homogeneous model has light calculation load and high practicability, it is widely applied in the field of industry. However, the models often provide false results even for simple flow around single hydrofoil [1], and they cannot predict quantitatively sheet cavitation inception from free nuclei due to their nature of homogeneous flow assumption. In popular cavitation models [2-5], model parameters such as number and radius of bubble nuclei and initial void fraction are used as tuning parameters to predict focused flow field with acceptable accuracy, whereas considerable gaps sometimes exist between the well-tuned values and actual ones. On the other hand, it has been confirmed through an experiment that behavior of sheet cavitation in growth stage as well as its inception is strongly affected by the number density distribution of bubble nuclei. Therefore, while it is hard to predict the inception of sheet cavitation, it is valuable to investigate the effects of the parameters regarding nuclei also by homogeneous approach.

The aim of this study is to evaluate the effects of the parameters, the number and the initial diameter of bubble nuclei, on global behavior of cavitating flow around an isolated Clark Y hydrofoil in numerical simulation. To obtain the number and the initial diameter of bubble nuclei, experimental measurements of the number density distributions of bubble nuclei are conducted in our cavitation tunnel. Then the numerical simulations are carried out using homogeneous cavitation model with different pairs of the

number and the radius of bubble nuclei; one of which is often used as default values in a popular cavitation model, and another is obtained values by the measurements to evaluate the effects of such parameters on global behavior of cavitating flow around a hydrofoil.

1. METHODS

1.1 Simulation methods

Two- and three-dimensional simulations are conducted for cavitating flow around a two-dimensional Clark Y-11.7% hydrofoil which has 100mm of chord length, c , as shown in Fig. 1. In three-dimensional simulations, the half of span (full span length, s , is 81 mm) is set assuming the flow symmetry. The analytical area is shown in Fig. 2. The inlet and outlet boundaries are located at $5c$ far from the center of the hydrofoil. The height of the area is $2c$, and the angle of attack of the hydrofoil is 8 degrees. The number of grid nodes is 230,000 for two-dimensional calculation or 3,800,000 for three-dimensional calculation. The vapor-liquid two-phase flow is treated as a homogeneous flow in which liquid-vapor mixture density is variable depending on void fraction but whose momentum is defined by an incompressible Navier-Stokes equation. The continuous equation, the momentum equation for the homogeneous flow, and the transport equation of vapor volume fraction are as follows, respectively, which are solved by ANSYS CFX 16.2,

$$\frac{\partial \rho_m}{\partial t} + \nabla \cdot (\rho_m \bar{u}_m) = 0, \quad (1)$$

$$\frac{\partial (\rho_m \bar{u}_m)}{\partial t} + \nabla \cdot (\rho_m u_m u_m) = -\nabla p + \nabla \cdot \mu_m (\nabla u_m + \nabla u_m^T), \quad (2)$$

$$\frac{\partial}{\partial t}(\alpha_v \rho_v) + \nabla \cdot (\alpha_v \rho_v \vec{u}_m) = S_v, \quad (3)$$

where \vec{u}_m , $\rho_m = \rho_l(1-\alpha_v) + \rho_v \alpha_v$, ρ_l , ρ_v , p , μ_m and α_v are the velocity for mixture, the densities of mixture, liquid and vapor phases, the pressure, the mixture viscosity and the vapor phase volume fraction, respectively. For the source term of transport equation of vapor volume fraction in two-dimensional simulation, S_v , two cavitation models, Schnerr-Sauer model (SS) [5] and Bubble-Droplet1 Viscosity Filtering model (BD1VF) developed by Yamamoto et al. [6], are employed, while only BD1VF is employed in three-dimensional simulation.

In SS the continuous phase is liquid, and the source term is expressed by

$$S_v = \text{sign}(p_v - p) C \frac{\rho_v \rho_l}{\rho_m} \alpha_v (1 - \alpha_v) \frac{3}{r} \sqrt{\frac{2|p_v - p|}{3\rho_l}}. \quad (4)$$

This term has been derived theoretically from the bubble dynamics with as an adjusting parameter C which should be the order of unity. In this study, $C=1$ is set.

BD1VF switches continuous phase depending on local void fraction. For the low void fraction region ($\alpha_v < 0.5$), the continuous phase is liquid, and mass source term is based on bubble dynamics as SS, while, for the high void fraction region ($\alpha_v > 0.5$), the continuous phase is vapor, and the source term is derived from Schrage's mass flux based on evaporation and condensation as Eq. (5),

$$S_v = \frac{k}{\sqrt{2\pi R_g T}} \frac{3(1-\alpha_v)}{r_{drop}} (p_v - p), \quad (5)$$

where R_g , T and k are the gas constant, temperature and evaporation-condensation coefficient ($=0.5$), respectively. The radii of bubble and droplet, r and r_{drop} , in Eqs. (4) and (5) are calculated from the expression of vapor volume fraction, $\alpha_v = (4\pi n_{nuc} r^3 / 3) / (1 + 4\pi n_{nuc} r^3 / 3)$, with the number of bubble nuclei per unit liquid volume, n_{nuc} , as follows,

$$r = \sqrt{\frac{\alpha_v}{\frac{4\pi}{3} n_{nuc} (1-\alpha_v)}}, \quad (6)$$

$$r_{drop} = \sqrt{\frac{1-\alpha_v}{\frac{4\pi}{3} n_{nuc} \alpha_v}}. \quad (7)$$

To evaluate the effects of the parameters regarding bubble nuclei, two pairs of n_{nuc} , and the initial diameter of nuclei, d_{nuc} , are used. One is often used as default values for SS in which n_{nuc} and d_{nuc} are $1.6 \times 10^{13} \text{m}^{-3}$ and $2.0 \times 10^{-6} \text{m}$, respectively. In addition, another pair obtained by the measurement of the

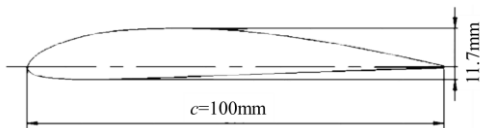


Figure 1. Clark Y-11.7% hydrofoil

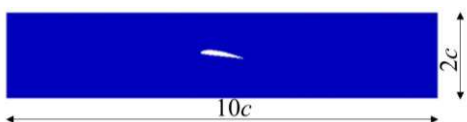


Figure 2. Computational domain

number density distribution of bubble nuclei is also used, which will be described later. Moreover, to improve reproducibility of cavitation unsteadiness, BD1VF cuts the eddy viscosity of the mixture using hyperbolic tangent to have gradual change in eddy viscosity as shown in Fig. 3. For turbulence model, $k-\omega$ SST model is employed for the two-dimensional simulation. As shown later, it gives us better agreement of pressure distribution in non-cavitating condition with experiment. However, in three-dimensional simulation, the model is found to overestimate the corner separations at the roots of the blade, resulting in the deviated pressure distribution. Thus, we have decided to use $k-\varepsilon$ model instead. We do not know why $k-\varepsilon$ model gives better result with less corner separations, but we have taken the reproduction of flow field for our priority. The time step is set to $1 \times 10^{-4} \text{s}$. The boundary conditions are set as shown in Table 1. The cavitation number, σ , the lift coefficient, C_L , the drag coefficient, C_D , and the pressure coefficient, C_p , are defined by the area-averaged pressure at 200mm upstream of the center of the blade, p_{ref} , and the velocity at 200mm upstream of the center of the blade, U_{in} , as follows,

$$\sigma = \frac{p_{ref} - p_v}{0.5 \rho_l U_{in}^2}, \quad (8)$$

$$C_L = \frac{F_L}{0.5 c s \rho_l U_{in}^2}, \quad (9)$$

$$C_D = \frac{F_D}{0.5 c s \rho_l U_{in}^2}, \quad (10)$$

$$C_p = \frac{p - p_{ref}}{0.5 \rho_l U_{in}^2}, \quad (11)$$

where ρ_l , p_v , F_L and F_D are the liquid density, the saturation pressure, the lift force and the drag force, respectively.

1.2 Bubble nuclei parameters

The cavitation tunnel used in this observation consists of a tank, a test section and a pump. The test section shown in Fig. 4 has a rectangular cross-section and a Clark Y-11.7% hydrofoil, which are basically identical to the configuration of the three-dimensional simulation. However, in the

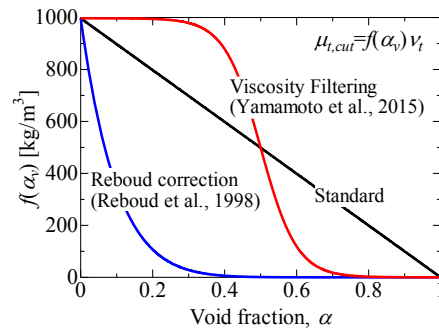


Figure 3. Viscosity Filtering

Table 1. Boundary conditions

Boundary	Condition
Inflow	$U_{in} = 8.2 \text{ m/s}$
Outflow	Constant
Upper and lower walls	Free slip wall
Blade surface	No slip wall
Side wall (3D)	No slip wall

experiment, there is 0.5mm of a tip clearance, which is not considered in the numerical simulation. The test section pressure, p_{ref} , is measured by a pressure transducer and is decreased stepwise from non-cavitation condition to super cavitation condition by a vacuum pump connected to the tank. In each stage, bubble nuclei are observed by a high-speed camera (Vision Research, Phantom V4.3) located at upstream from the center of the blade as shown in Fig. 4. The camera settings are summarized in Table 2. The backlighted images are recorded, and the measurements of the number density distributions are conducted by image processing. In addition to this observation, F_L and F_D are measured under the assumption of two-dimensional flow by strain gauges attached to cantilevered beam supporting the hydrofoil with the sampling frequency and the sampling time of 1000Hz and 40s, respectively. The dissolved air in water is evaluated by the Dissolved Oxygen (DO) which is measured before and after the experiments. In this observation and measurement, DO is approximately 1.3mg/L (20%), and U_{in} is set to 8.2m/s.

Figure 5 shows the measured number density distributions of bubble nuclei, $N(r)$, where r is radius of nuclei. It can be seen that the number density is increased at $\sigma=0.51$. Since the cavitation tunnel is a closed loop one, bubbles generated by cavitation circulate, and the number density starts to increase at around $\sigma=0.5$ which is close to the saturation condition of DO ($\sigma_{DOsat}=0.4$). To determine the parameter of n_{nuc} and d_{nuc} for this simulation, the approximation formula for $N(r)$ is obtained from the number density distributions as shown in Fig. 5 and is expressed as follows,

$$\log N(r) = -3.5 - 3 \log r. \quad (12)$$

The pressure coefficient at the suction peak on the blade surface, C_{pmin} , is found to be around -3.5 from numerical simulation of single phase flow. The radius of nuclei, r_{ref} , which quasi-statically grows to the critical radius at C_{pmin} with the inlet pressure, p_{ref} , is calculated by Laplace formula. Then n_{nuc} and d_{nuc} are obtained as follows,

$$n_{nuc} = \int_{r_{ref}}^{\infty} N(r) dr, \quad (13)$$

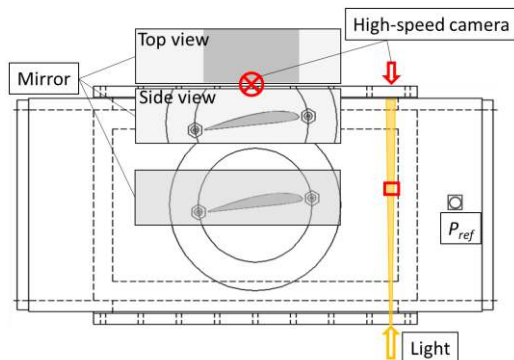


Figure 4. Test section

Table 2. Camera settings for nuclei observations

Resolution [pixels]	256 x 512
Spatial resolution [$\mu\text{m}/\text{pixel}$]	6
Depth of field [mm]	4
Frame rate [fps]	4000
Exposure time [μs]	10
Recording time [s]	1

$$d_{nuc} = \frac{2}{n_{nuc}} \int_{r_{ref}}^{\infty} r N(r) dr. \quad (14)$$

In this simulation, the inlet pressure at inception ($\sigma=1.8$) is used for p_{ref} , and as a result, 3.3×10^{-6} m for d_{nuc} , and 2.4×10^8 m^{-3} for n_{nuc} are obtained. The order of the obtained d_{nuc} is similar to that of the default value, whereas the order of n_{nuc} is much smaller than the default value by 5. These obtained and default pairs of n_{nuc} and d_{nuc} are applied to the simulations, and the results are compared.

2. RESULTS AND DISCUSSION

The pressure distributions on the blade suction surface which are time-averaged for 0.5s are shown in Fig. 6 for the two-dimensional simulations with (a) SS and (b) BD1VF, and for (c) the three-dimensional simulation with BD1VF. The time-averaged pressure distribution obtained by experiments (Matsunari et al. [7]) is also plotted in Fig. 6. Time-averaged lift coefficient, C_L , are shown in Fig. 7 for the three-dimensional simulation and the two-dimensional simulations with SS and BD1VF. In the non-cavitation condition ($\sigma=3.5$), the pressure distributions of the simulations well agree with the experimental data. In C_L in non-cavitation condition shown in Fig. 7, although there is a gap between the simulation results and the experimental data approximately 0.3, C_L in the non-cavitation condition for the three-dimensional simulation is slightly smaller than that for the two-dimensional simulation. This difference is caused by the end wall effects in three-dimensional simulation. In the discrepancy of approximately 0.3 between experiment and simulations, it seems to be caused by asymmetry of the flow due to existence of tip clearance in the experiment; the tip clearance should be arranged for measurement of C_L , which produces bending moment and displaces the working point of the lift force from the center of the blade in the spanwise direction. However, C_L is measured under the assumption of asymmetric flow and the neglect of the bending moment.

In the cavitating condition ($\sigma=1.8$) of the two-dimensional simulation with SS, the pressure in the region covered by cavity is almost equal to the vapor pressure for the both cases of large and small numbers of nuclei. However, the vapor pressure region in the case of the small number of nuclei is larger. In the two-dimensional simulation results with BD1VF,

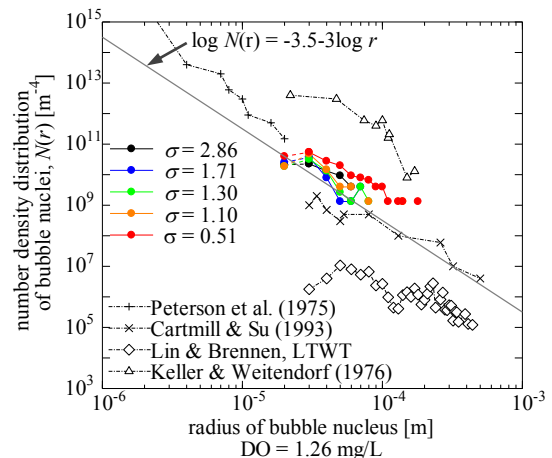


Figure 5. Number density distribution of bubble nuclei

the pressure in the cavitating region is again almost equal to the vapor pressure. However, compared with SS simulation, the pressure recovery behind the cavity region is gradual, and it is more gradual with the large number of nuclei than that with the small number of nuclei. The reason for this is probably due to the unsteadiness of cavitation. In the simulation with BD1VF, the fluctuation of the cavity length is more remarkable as will be seen later. The time averaged pressure near the fluctuating cavity trailing edge takes larger value than vapor pressure, resulting in the above-mentioned gradual pressure recovery near the cavity trailing edge.

In three-dimensional simulation, the pressure inside the cavity region is almost constant at the vapor pressure as it is in the two-dimensional simulation with BD1VF. However, even with BD1VF model, the pressure recovery behind the cavity is rather steep, indicating that the unsteadiness of cavitation is weaker than that in two-dimensional simulation. The cavity length (area of vapor pressure) is almost similar in the cases with the large and small numbers of nuclei. However, looking at the leading edge area more closely, the suction pressure peak can be recognized especially in the case with the small number of nuclei. From Eqs. (4) and (5), since the vaporization speed for the small number of nuclei is slower than that for the large number of nuclei and the nuclei around the suction peak are in the growth stage, then the pressure around the suction peak can be kept lower than the vapor pressure.

The instantaneous cavity shapes of the two-dimensional simulations in the case of $\sigma=1.8$ are shown for SS in Fig. 8 and for BD1VF in Fig. 9. The cavity is visualized by the numerical elements colored with the local void fraction larger than 0.1. The corresponding total void volume and C_L fluctuations are shown in Fig. 10. The total void volume is calculated by volume integral of α_v over the whole computational volume. As shown in Fig. 8, cloud cavities are not observed in SS, while the total void volume and C_L fluctuate periodically. The frequencies of the void volume and C_L fluctuations are close to each other, while the amplitude is apparently larger in the large number of nuclei than that in the small number of nuclei. Therefore, it is suggested that the frequencies are related to fluctuation of cavity length, and the amplitudes are to the magnitude of cavity volume fluctuation. On the other hand, in BD1VF simulation in Fig. 9, cloud cavities are observed in the both large and small numbers of nuclei. In Fig. 10(b) for the large number of nuclei, two frequency components can be recognized. One is similar to the frequency of elongating and shrinking motion observed in SS simulation, and another is high frequency component related to cloud cavity shedding. In the small number of nuclei, the void volume and C_L fluctuate mainly in response to cloud cavity shedding. In the small number of nuclei, the cavity volume is smaller than that of the large number of nuclei, and therefore the component of the fluctuation of cavity length is unremarkable.

The instantaneous cavity shapes and C_L fluctuations for the three-dimensional simulation are shown in Figs. 11 and 12, respectively. The cavitation number is $\sigma=1.9$. In the three-dimensional simulation, unsteadiness of cavitation is weaker than that in the two-dimensional simulation. The size of cavitation region looks similar between the large and small

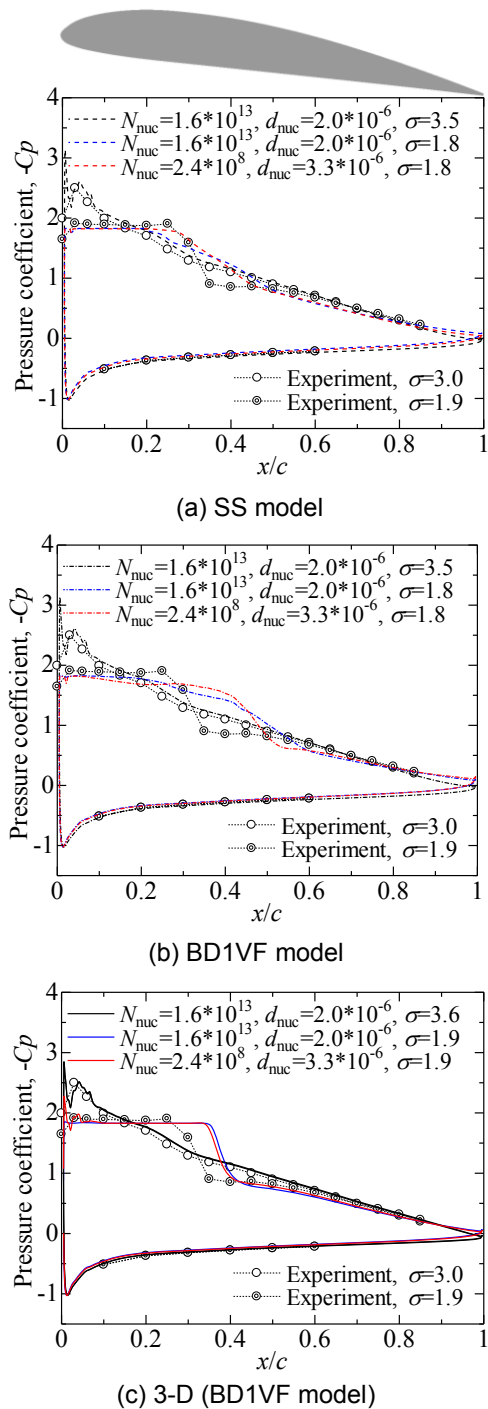


Figure 6. Pressure distributions on hydrofoil surface

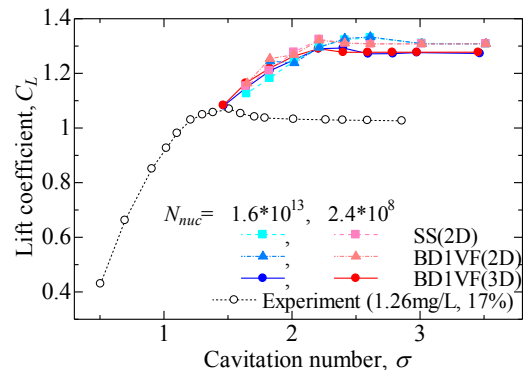


Figure 7. Lift coefficients

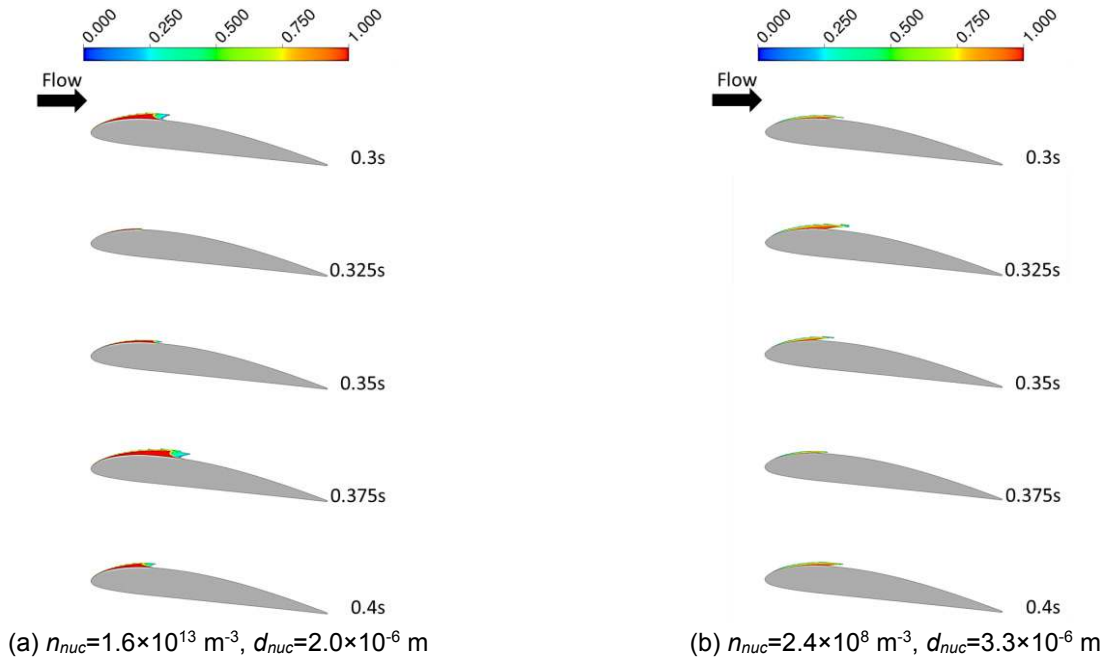


Figure 8. Instantaneous void fraction distributions in the two-dimensional simulation with SS ($\sigma=1.8$)

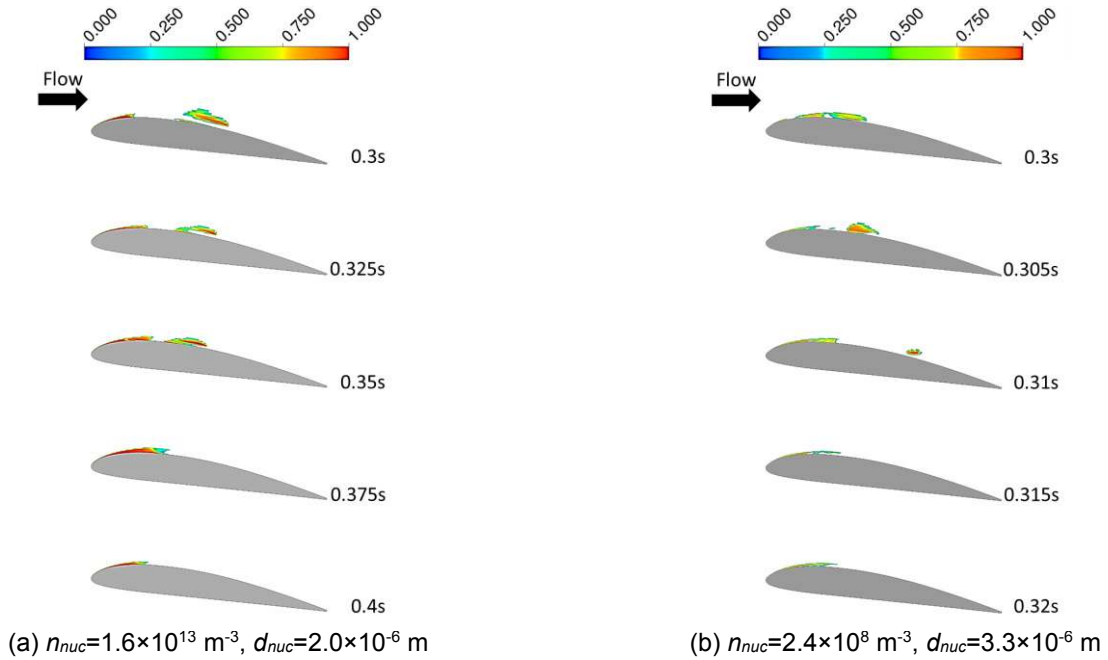


Figure 9. Instantaneous void fraction distributions in the two-dimensional simulation with BD1VF ($\sigma=1.8$)

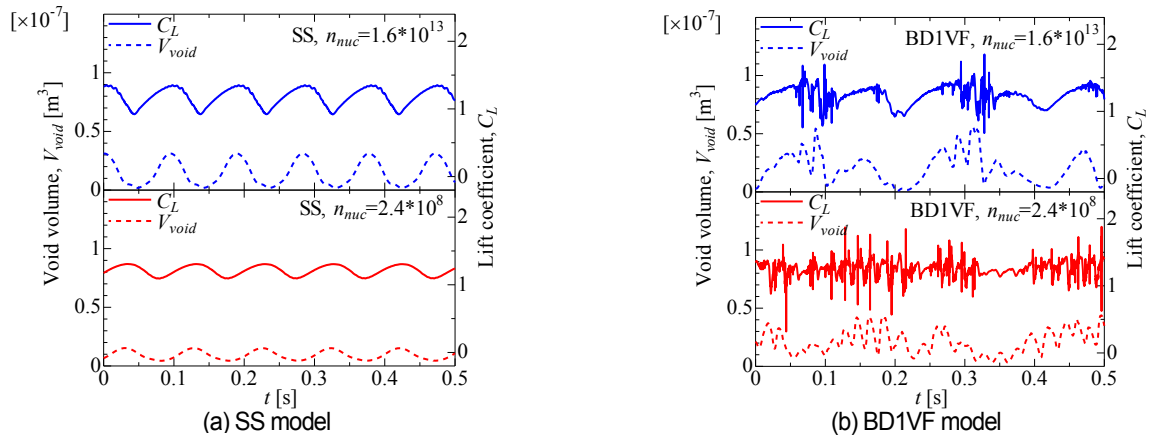


Figure 10. Lift coefficient and void volume fluctuations in the two-dimensional simulations ($\sigma=1.8$)

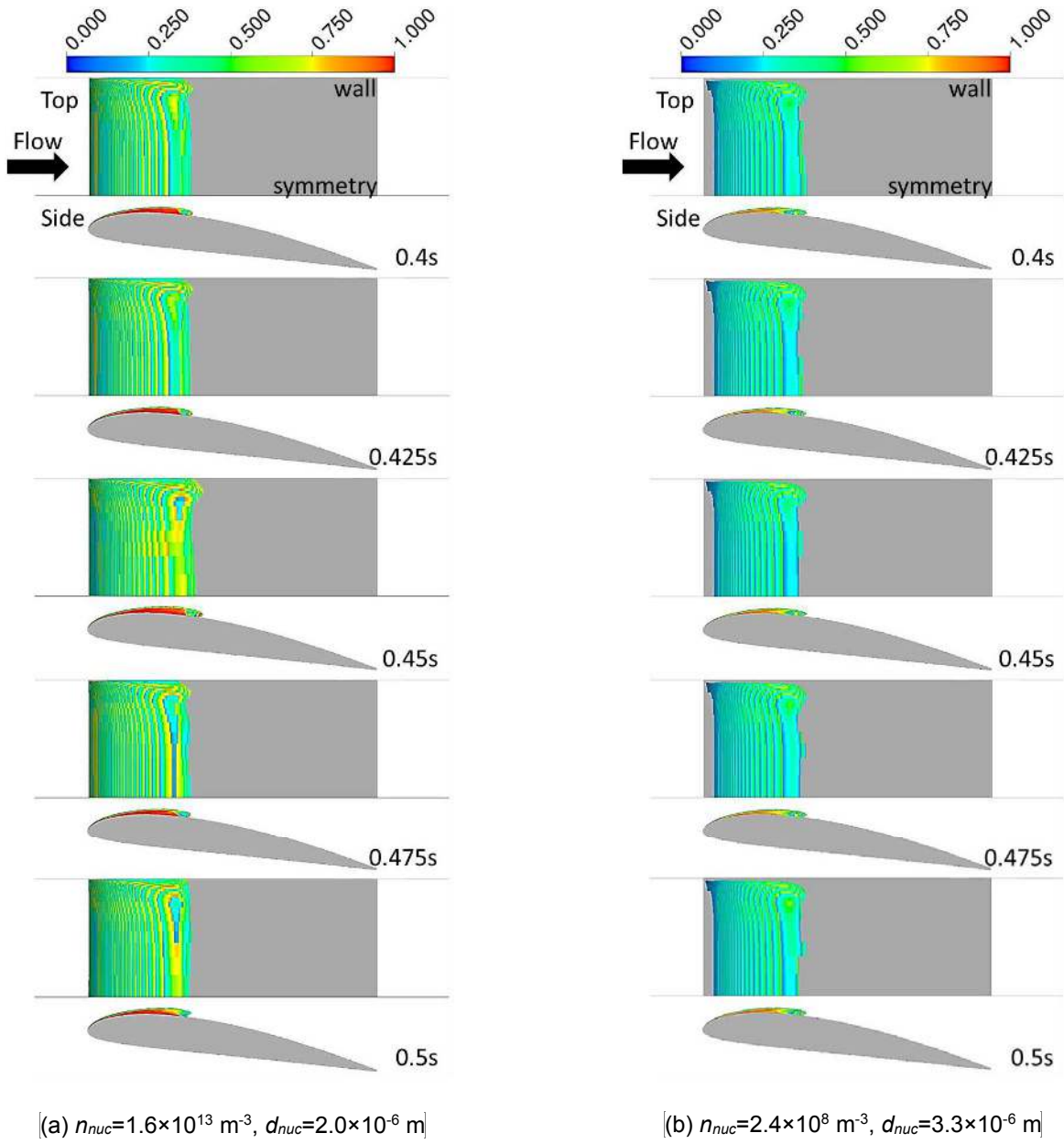


Figure 11. Instantaneous void fraction distributions in the three-dimensional simulation with BD1VF ($\sigma=1.9$)

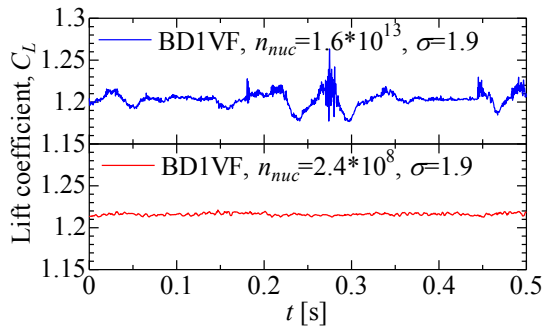


Figure 12. Lift coefficients fluctuation in the three-dimensional simulation with BD1VF ($\sigma=1.9$)

numbers of nuclei, but the actual time-averaged volumes of cavity are different; $1.5 \times 10^{-6} \text{ m}^3$ in the large number of nuclei while $9.4 \times 10^{-7} \text{ m}^3$ in the small number of nuclei. In the both cases with the large and small numbers of nuclei, the three-dimensionality of the cavity shape can be seen near the side wall. Since the void volume in the large number of nuclei is larger than that in the small number of nuclei, the amplitude of C_L fluctuation in the large number of nuclei is larger. In the both large and small numbers of nuclei, the location of the cavity trailing edge are almost the same. However, the cavity leading edge for the small number of nuclei is located relatively downstream. As already mentioned, since the vaporization speed for the small number of nuclei is slower than that for the large number of nuclei, nuclei are still in a growth stage around the suction peak. In reality, the sheet

cavity leading edge is not located at the suction peak but is often located near a separation point or a re-attachment point downstream of the suction peak where free nuclei attach to the wall and grow to sheet cavity [8]. This indicates that the inception of sheet cavitation involves some heterogeneous processes. In the simulations based on the homogeneous model, nuclei exist everywhere, and they can grow at any locations with the low pressure below the vapor pressure. Even with this difference, the location of cavity leading edge in the simulation using the number of nuclei obtained by actual number density distribution of nuclei is closer to that in the actual sheet cavitation.

3. CONCLUSION

The two different pairs of parameter regarding bubble nuclei are applied to the homogeneous flow simulation, and the effects of characteristics of bubble nuclei on cavitating flow are investigated. The frequencies and amplitudes of fluctuations of the lift coefficient and cavity volume are affected by the number of bubble nuclei. Although the actual inception of sheet cavitation involves some heterogeneous process, the cavity leading edge and the pressure distribution around suction peak are well simulated by the present homogeneous simulation using the number of nuclei obtained by experimental measurement. This seems to indicate the possibility of the further improvement of homogeneous cavitation model in prediction accuracy.

ACKNOWLEDGMENTS

This study is partly supported by JSPS KAKENHI Grant Number JP17J04154.

REFERENCES

- [1] C. Kato, Industry-university collaborative project on numerical predictions of cavitating flows in hydraulic machinery – part I: Benchmark test on cavitating hydrofoils -, Proc. ASME-JSME-KSME Joint Fluids Engineering Conference 2011, AJK2011-06084 (2011).
- [2] R. F. Kunz, D. A. Boger, D. R. Stinebring, T. S. Chyczewski, J. W. Lindau, H. J. Gibeling, S. Venkateswaran and T. R. Govindan, A Preconditioned Navier-Stokes Method for Two-Phase Flows with Application to Cavitation Prediction, Computers & Fluids, Vol. 29, pp. 849-875 (2000).
- [3] C. L. Merkle, K. Feng, and P. E. Below. Computational Modeling of the Dynamics of Sheet cavitation. Proc. the 3rd International Symp. on Cavitation, Grenoble, France, Vol. 2, 47-54, (1998).
- [4] P. K. Zwart, A. G. Gerber and T. Belamri, A Two-Phase Flow Model for Predicting Cavitation Dynamics, Proc. the Fifth Int. Conf. on Multiphase Flow, (2004).
- [5] G. Schnerr and J. Sauer, Physical and Numerical Modeling of Unsteady Cavitation Dynamics. Proc. Fourth International Conference on Multiphase Flow, (2001).
- [6] Y. Yamamoto, S. Watanabe and S. Tsuda, A Simple Cavitation Model for Unsteady Simulation and its Application to Cavitating Flow in Two-Dimensional Convergent-Divergent Nozzle. IOP Conf. Ser.:Mater. Sci. Eng. 72:022009, (2015).
- [7] H. Matsunari, S. Watanabe, Y. Konishi, N. Suefuji, A. Furukawa, Experimental/Numerical Study on Cavitating Flow around Clark Y 11.7% Hydrofoil, Proc. the 8th International Symposium on Cavitation, (2012).
- [8] M. Rijsbergen, A Review of Sheet Cavitation Inception Mechanisms, Proceedings of ISROMAC2016, No. 356, (2016).

Nomenclature

Roman symbols

C	Coefficient in Schnerr-Sauer model
C_D	Drag coefficient
C_L	Lift coefficient
c	Cord length
d_{nuc}	Diameter of nuclei
F_D	Drag force
F_L	Lift force
k	Evaporation-condensation coefficient
N	Number density distribution function
n_{nuc}	Number of nuclei par unit liquid volume
p	Pressure
R_g	Gas constant
r	Radius of bubble
r_{drop}	Radius of droplet
S_v	Source term
s	Span length
T	Temperature
t	Time
U_{in}	Inlet velocity
u	Velocity

Greek symbols

α	Void fraction
μ	Viscosity
ρ	Density
σ	Cavitation number

Subscripts

l	Liquid phase
m	Mixture
p	Pressure
ref	Reference
v	Vapor phase